INTERNATIONAL ATOMIC ENERGY AGENCY
UNITED NATIONS EDUCATIONAL, SCIENTIFIC AND CULTURAL ORGANIZATION

INTERNATIONAL CENTRE FOR THEORETICAL PHYSICS
34100 TRIESTE (ITALY) - P.O.B. 586 - MIRAMARE - STRADA COSTIERA 11 - TELEPHONE: 2240-1
CABLE: CENTRATOM - TELEX 460392 - I

H4.SMR/285 - 36

WINTER COLLEGE ON
LASER PHYSICS: SEMICONDUCTOR LASERS
AND INTEGRATED OPTICS

(22 February - 11 March 1988)

INTEGRATED OPTICAL PASSIVE DEVICES

W. Sohler
Angewandte Physik
Universität-GH-Paderborn
F.R. Germany

W. Sohler
Angewandte Physik
Universität-GH-Paderborn

INTEGRATED OPTICAL PASSIVE DEVICES

- WAVEGUIDES
- COUPLERS
- LENSES
- PRISMS
- POLARIZERS
- TE/TM - MODE SPLITTER
- BEAM SPLITTER
- GRATING DEVICES (FILTER ETC.)
- MIRRORS
- .....

Beam couplers

i) transversal coupler (end-fire coupling)

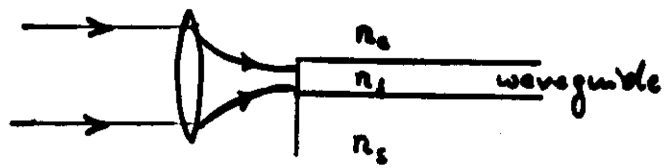

$$\eta = \frac{\left[\int E_L(x,y)\, E_{wg}^{*}(x,y)\, dx\, dy\right]^2}{\int |E_L(x,y)|^2 dx\, dy \int |E_{wg}(x,y)|^2 dx\, dy}$$

ii) prism coupler

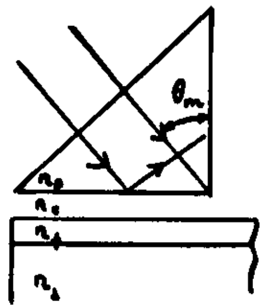

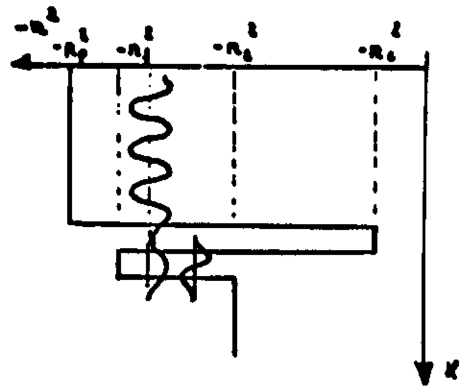

$\beta_m = \frac{\omega}{c} n_p \sin\theta_m$

"optical tunneling"

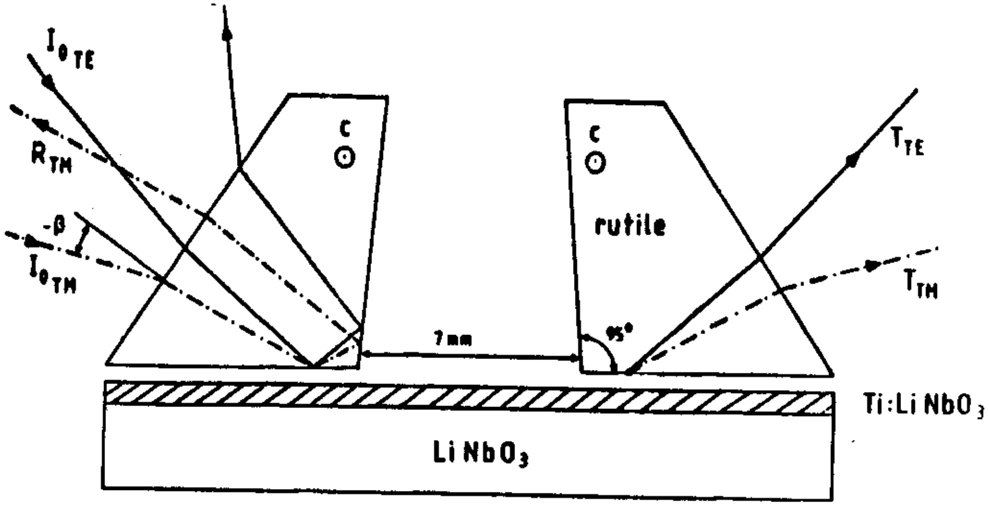

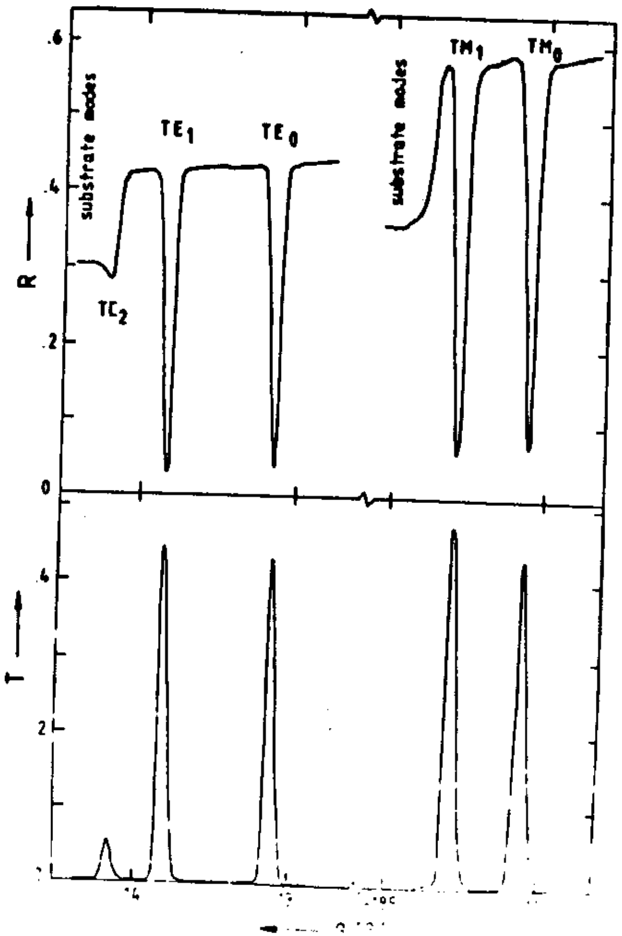

after: Soller + Sude

iii) grating coupler
(after Tien)

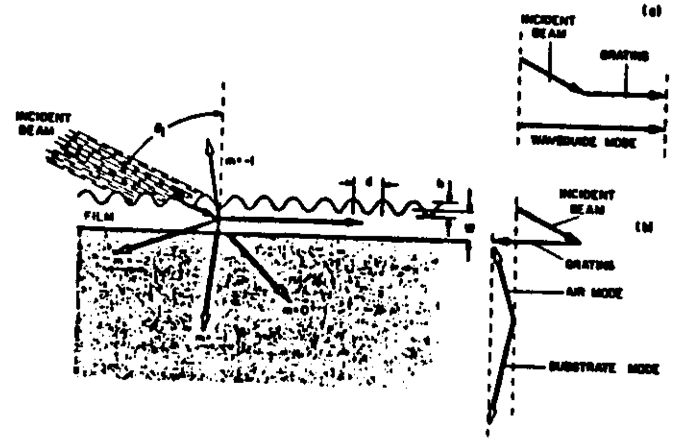

FIG. 13. The figure at the left shows how a grating can diffract an incident wave into many orders. A zigzag wave and thus a "waveguide" mode is excited in a waveguide only if one of the diffraction orders is in phase with the zigzag wave. The diagram in (a) shows the vector relation required for such a grating coupler. On the other hand, other diffraction orders of the grating could match the phases of the "substrate" or "airspace" modes and thus introduce losses to the coupling by diverting part of the incident energy into radiations in substrate or airspace.

iv) taper coupler

(Tien)

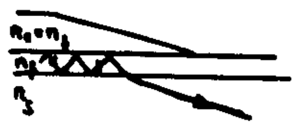

(Soller)

Integriert optische Linsen

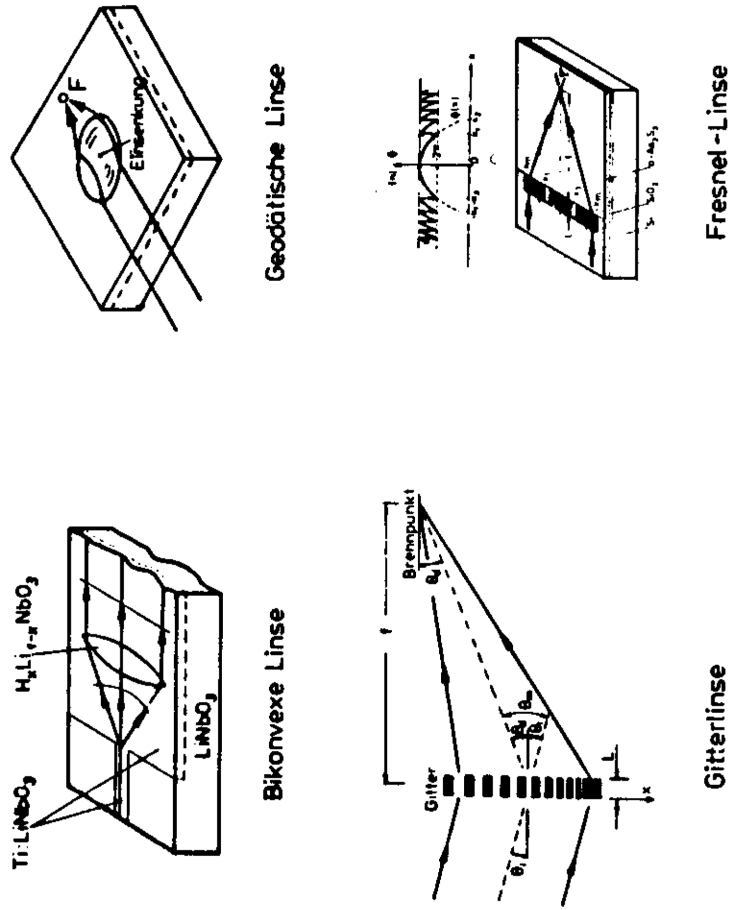

grating lens:

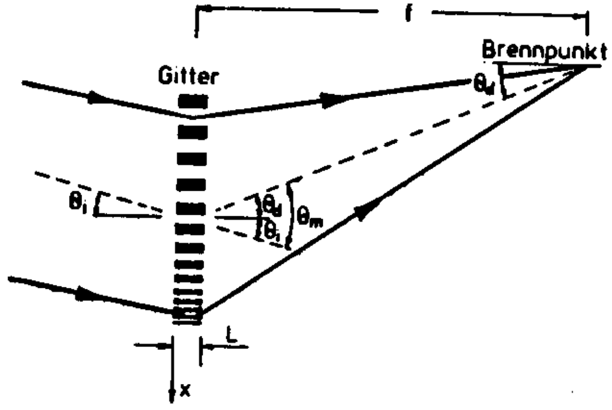

wave vectors:

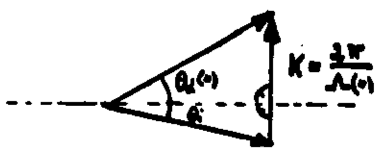

$$K = \frac{2\pi}{\Lambda(x)}$$

$$\frac{2\pi}{\lambda} n_{eff} \left(\sin\theta_i + \sin\theta_d(x) \right) = \frac{2\pi}{\Lambda(x)}$$

$$\Rightarrow \quad \Lambda(x) = \frac{\lambda}{n_{eff} \left(\sin\theta_i + \sin\theta_d(x) \right)}$$

with $x = f \tan\theta_d$

experimental example:
(after Yao et al.)

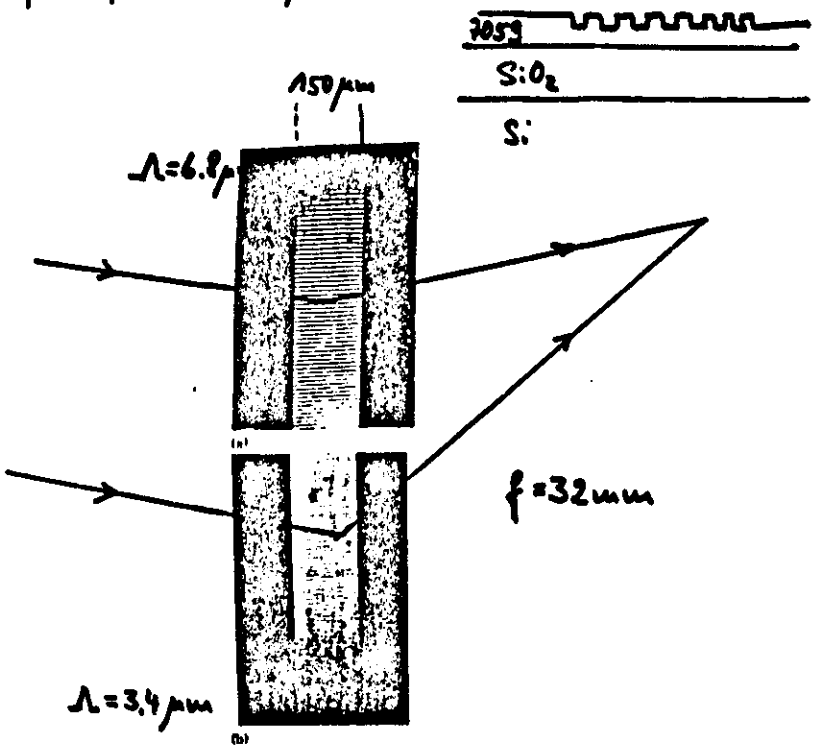

FIG. 2. The chromium master mask for the chirp-grating lens. (a) Low-frequency portion; (b) High-frequency portion.

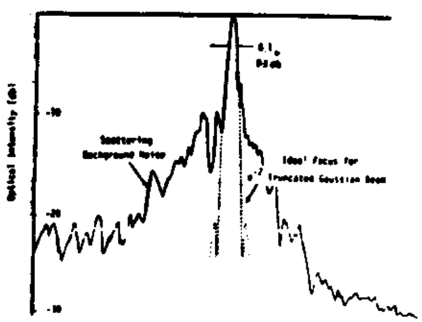

FIG. 4. Measured focal spot of the chirp-grating lens.

Fresnel Lens

convent. lens: $\phi(x) \approx -\frac{2\pi}{\lambda} n \frac{1}{2f} x^2$

Fresnel lens: $\phi_F(x) \approx -\frac{2\pi}{\lambda} n_{eff} \frac{1}{2f} x^2 + m \cdot 2\pi$

with $-2\pi < \phi_F(x) < 0$ $\qquad m = 1, 2, \ldots$

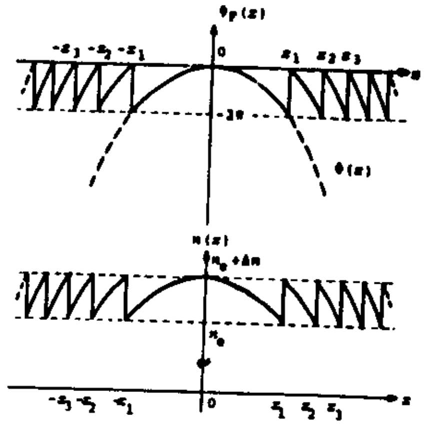

Fig 2 Phase modulation $\Phi(z)$, $\Phi_F(z)$, and mode-index distribution $\Delta n(z)$ of a GRIN Fresnel waveguide lens.

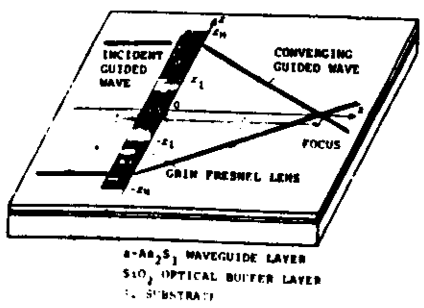

Fig 1 Graded index Fresnel waveguide lens configuration

experimental example: after Valette et al.

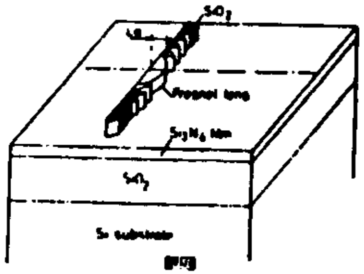

Fig. 1 Schematic drawing of integrated analogue Fresnel lens

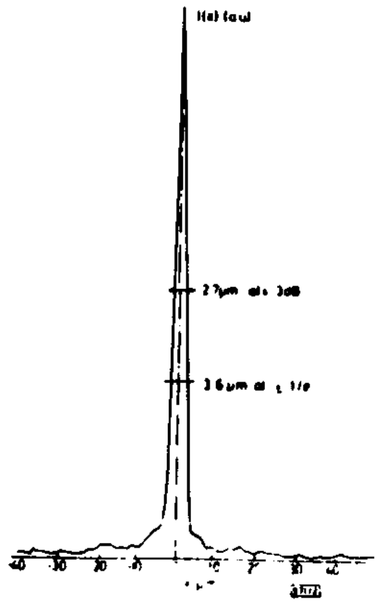

Fig. 2 Typical light distribution in focal line [illegible] input beam

geodesic lenses:

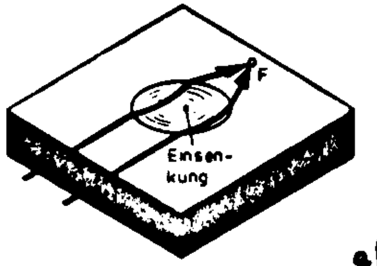

after Schulz + Voges

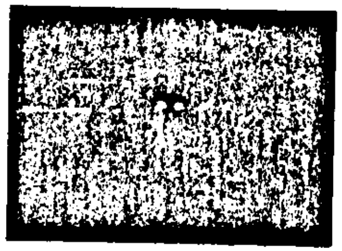

after Righini et al.

Luneburg-lens:

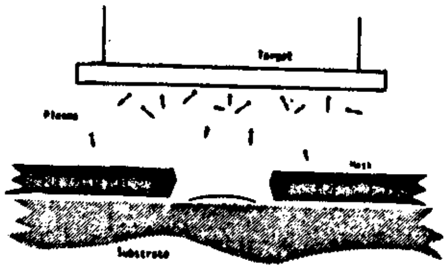

FIG. 1. Shadow mask sputtering configuration.

experimental example: after Yao et al.

Ta_2O_5 lens on 7059 waveguide on SiO_2 substrate

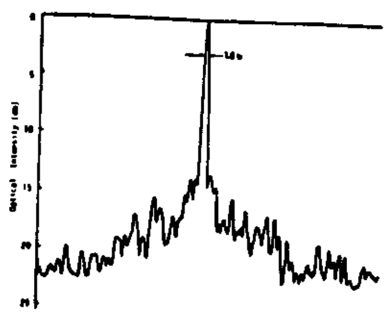

FIG. 3. Measured focal intensity pattern for an F/4 waveguide Luneburg lens with a 8-mm lens diameter and a 8-mm focal length, using a 2-mm aperture.

"Conventional" lens:

in $LiNbO_3$ by proton exchange
(see Tsai et al.)

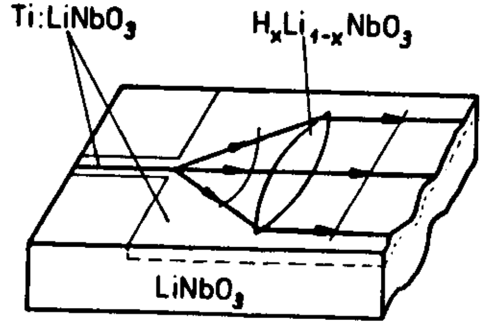

prism: see slide

polarizer:

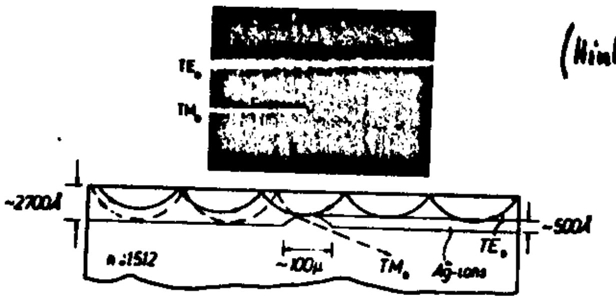

(Hinkov + Sohler)

reduced depth polarizer

(Rollke + Sohler)

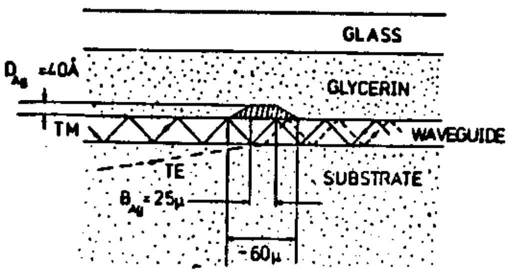

metal stripe polarizer

grating devices:

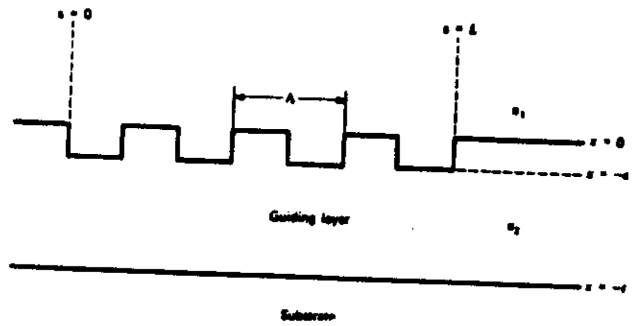

wave equation:

$$\nabla^2 E - \frac{n^2(x,y)}{c^2}\frac{\partial^2}{\partial t^2}E = \mu_0 \underbrace{\frac{\partial^2}{\partial t^2} P_{d}}_{\frac{\Delta n^2}{c^2}\frac{\partial^2}{\partial t^2}E}$$

ansatz: $E = \sum A_m(z)\, E_m(x,y)\, \exp\left[i(\omega t - \beta_m z)\right]$

coupling of two modes:

$$A_1'(z) = \varkappa_{12}\, A_2(z)\, e^{-i\Delta\beta z}$$
$$A_2'(z) = \varkappa_{21}^*\, A_1(z)\, e^{+i\Delta\beta z}$$

coupled mode theory (see: Yariv)

with: $\Delta\beta = \beta_1 - \beta_2 - K$

$\varkappa_{12} \sim \int \Delta n^2(x,z)\, E_1(x,y)\, E_2^*(x,y)\, dx\, dy$

solutions for $\Delta\beta = 0$:

$$A_1(z) = A_2(0)\,\frac{K_{12}}{|K_{12}|}\,\frac{\sinh[\varkappa(z-L)]}{\cosh(\kappa L)}$$

$$A_2(z) = A_2(0)\,\frac{\cosh[\varkappa(z-L)]}{\cosh(\kappa L)}$$

$\varkappa = |\varkappa_{12}|$

reflection: $\beta_2 = -\beta_1 \Rightarrow 2\beta_1 = K = \frac{2\pi}{\Lambda}$

$$\Rightarrow \boxed{\Lambda = \frac{\lambda}{2 n_{eff}}}$$

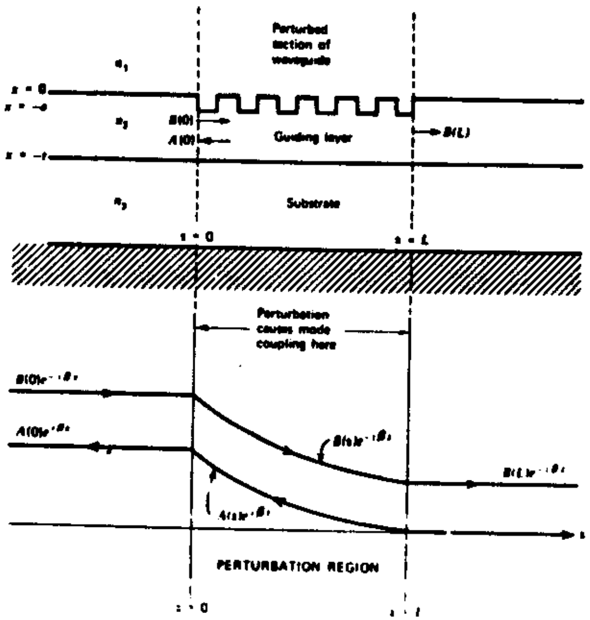

Figure 19.5 Upper: A corrugated Section of a dielectric waveguide. Lower. The incident and reflected fields.

$$\beta \approx \frac{\pi}{\Lambda} \pm i\left[K^2 - \left(\frac{n_{eff}}{c}\right)^2 (\omega-\omega_0)^2\right]^{1/2}$$

with $\omega_0 = \frac{\pi c}{\Lambda n_{eff}}$

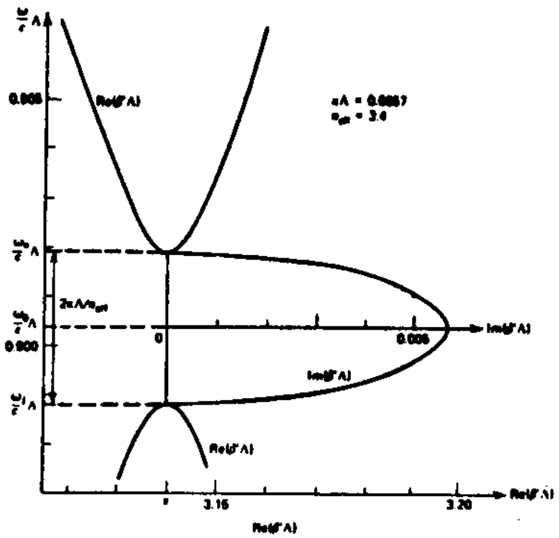

Figure 19.6 The dependence of the real and imaginary parts of the mode propagation constant, β', of the modes in a periodic waveguide near the first "forbidden" gap ($l = 1$). At frequencies $\omega_1 < \omega < \omega_u$, $\mathrm{Im}(\beta') \neq 0$ and the modes are evanescent. At these frequencies, Re $\beta' = \pi/\Lambda$. For $\varphi \neq 1$ the abscissa should be taken as $\mathrm{Re}(\beta'\Lambda/\varphi 0)$.

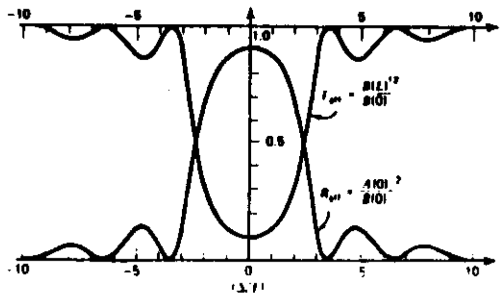

Figure 19.7 The transmission and reflection characteristics of a corrugated section of length L as a function of the detuning $\Delta\beta L$ [illegible] ($\kappa L = 1.84$)

planarer WL: LPE, InGaAsP mit $\lambda_g = 1.1\,\mu m$
6-7 dB/cm bei $\lambda \approx 1.5\,\mu m$

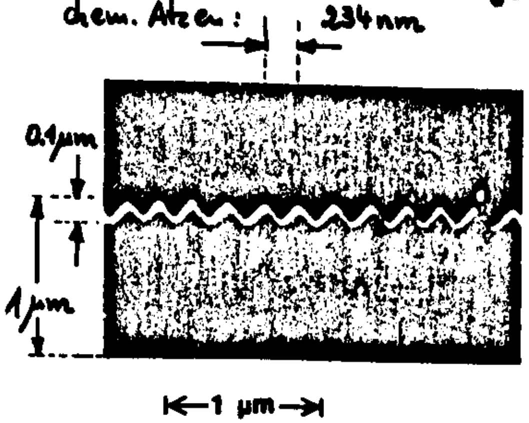

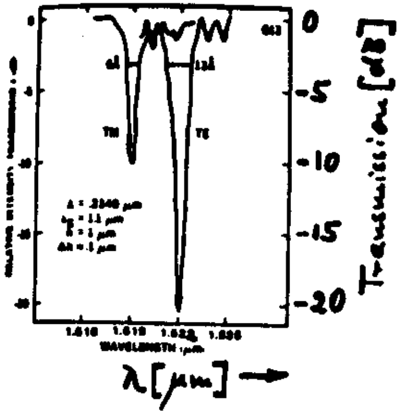

nach Alferness + ... (Bell), 1984

Resonator-Filter:

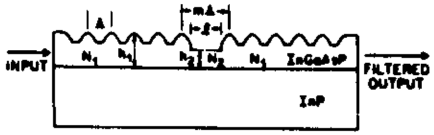

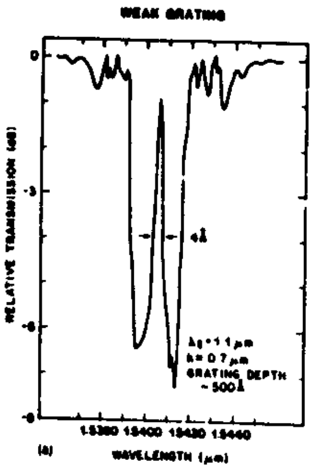

$(1\,Å \triangleq 13\,GHz)$

nach Alferness + .. (Bell), 1986

multiplexer / demultiplexer:

(after: Rottmann + Voges)

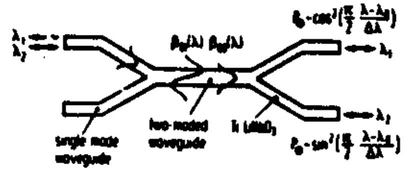

Fig. 1
Configuration of an integrated-optical dual-channel multiplexer/demultiplexer

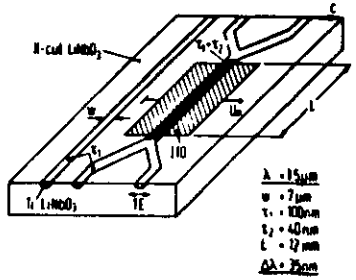

Fig. 2
Geometry of fabricated WDM-devices

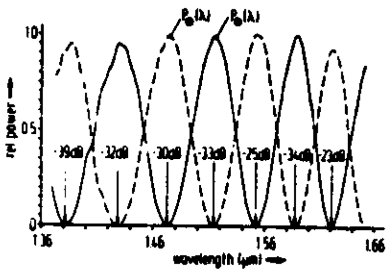

Fig. 3
Transmission characteristic of a dual-channel multiplexer/demultiplexer
Ti strip width 7 µm,
Ti thickness
100 nm + 40 nm,
L = 12 mm, TE pol.

mirrors:

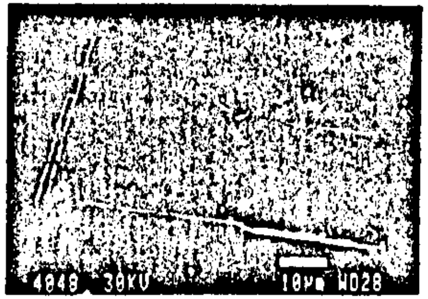

Fig.3 Reactive ion etched rib waveguides with totally reflecting corner mirror

etched mirror

(Buchmann et al.)

(n/n^+ - GaAs waveguide

evaporated end face mirror (see slide)

resonators: see modulators

beam splitters:

bulk optics:

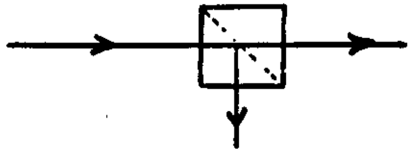

integrated optics:

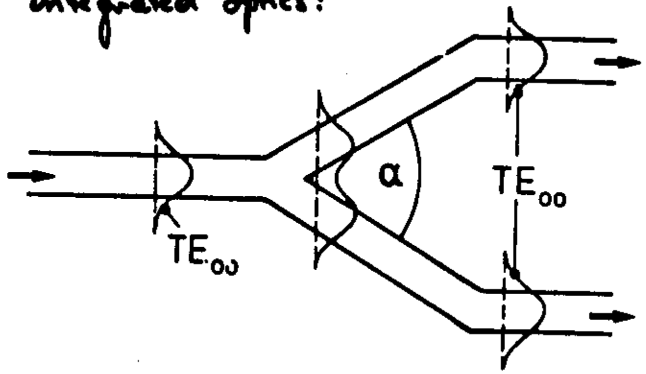

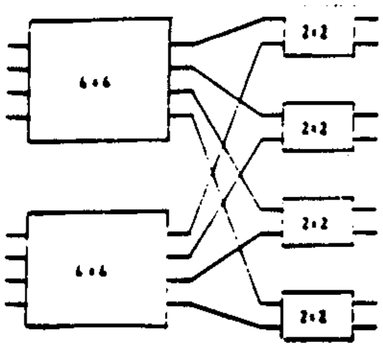

Star coupler:

Fig. 1: Architecture of the 8x8 star coupler

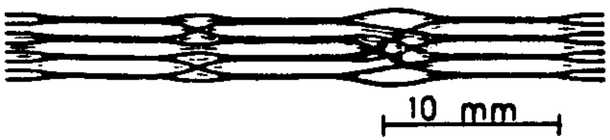

Fig. 2: 8x8 star coupler design

(after: Döldissen et al.)